Processing and Application of Ceramics 15 [1] (2021) 47–57
https://doi.org/10.2298/PAC2101047W



# Doping effects in $(Ba_{0.85}Ca_{0.15})(Hf_{0.1}Ti_{0.9})O_3$ lead-free piezoelectric ceramics prepared via powder injection moulding using simple binder

Can Wang[1], Bijun Fang[1,*], Shuai Zhang[1], Xiaolong Lu[1], Jianning Ding[1,2,*]

[1]*School of Materials Science and Engineering, Jiangsu Collaborative Innovation Center of Photovolatic Science and Engineering, Jiangsu Province Cultivation Base for State Key Laboratory of Photovoltaic Science and Technology, National Experimental Demonstration Center for Materials Science and Engineering, Changzhou University, Changzhou 213164, China*

[2]*School of Mechanical Engineering, Jiangsu University, Zhenjiang 212013, China*

Received 12 September 2020; Received in revised form 26 November 2020; Accepted 1 February 2021

## Abstract

*To improve densification of the $(Ba_{0.85}Ca_{0.15})(Hf_{0.1}Ti_{0.9})O_3$ (BCHT) ceramics prepared via powder injection moulding, $MnO_2$ and $Li_2CO_3$ were used as sintering aids. The BCHT ceramics doped with different Mn- and Li-amount prepared by powder injection moulding in which paraffin was used as injection binder, have rather pure perovskite structure with complicated polymorphic ferroelectric phase coexistence. Polyhedral grains combined with nearly round shape grains with increased relative density and larger gains size were obtained at appropriate doping amount, related to the formation of liquid phase during sintering and increased mobility of ions due to the generation of point defects caused by heterovalent cations doping. The Mn- and Li-doped BCHT ceramics are displacement driven ferroelectrics with apparent diffused transition characteristic at different extent, relating to the morphotropic phase boundary composition and the variation of point defects induced by doping. Comparable or surpassing electrical performance was acquired, especially the dielectric breakdown strength was increased due to the improved sinterability. With appropriate doping amount, piezoelectricity larger than 300 pC/N can be obtained in the Mn- and Li-doped BCHT ceramics poled under low electric field.*

***Keywords:*** *BCHT, powder injection moulding, paraffin, sintering aid, electrical properties*

## I. Introduction

$Pb(Zr_{1-x}Ti_x)O_3$ (PZT)-based perovskite ferroelectrics have monopolized world-wide commercial piezoelectricity-related applications, such as sensors, actuators, transducers, etc. due to the versatile excellent performance [1–3]. Due to the toxicity of lead, environmental protection and health concerns have excited booming requirements for lead-free perovskite piezoelectrics with competitive properties [4–6].

Recently, three categories of $BaTiO_3$ (BT)-based lead-free piezoceramics $(BaCa)(B'Ti)O_3$ (BCB'T, B' = Zr, Sn, Hf) have attracted extensive research interest since their piezoelectricity can catch up with or surpass that of the PZT-based piezoelectric ceramics [7–9]. The increased piezoelectricity-related physical mechanism was illuminated as construction of the triple critical point morphotropic phase boundary (TCP-MPB), where ferroelectric rhombohedral and tetragonal phases, and paraelectric cubic phase converged and formed phase boundary tiled to temperature axis [4,10,11]. The intermediate bridging ferroelectric orthorhombic phase was immediately observed, which provided more spontaneous polarization directions, degenerated the energy barrier for domains movement and switching, and played important role in such enhancement [4,10–12]. In the BCB'T system, $(BaCa)(HfTi)O_3$ ceramics attracted our research attention since rather high Curie temperature ($T_C$) can be obtained in the Hf-based solid solution [12,13].

Normally, the $(BaCa)(HfTi)O_3$ ceramics were prepared by solid-state sintering method and the sintering temperature was 1450 °C or above to obtain

* Corresponding author: tel: +86 519 86330095,
e-mail: *fangbj@cczu.edu.cn* (Bijun Fang)
*dingjn@cczu.edu.cn* (Jianning Ding)

high piezoelectric performance [8,10,13]. Since ceramics processing affects physical properties greatly [14–16], in our previous work [17] we prepared $(Ba_{0.85}Ca_{0.15})(Hf_{0.1}Ti_{0.9})O_3$ (BCHT) ceramics via powder injection moulding process using polyethylene glycol, polyvinyl butyral and polyoxymethylene as injection binders. Although improved electrical properties were obtained, the used injection binder system was complex and processing (including internal mixing, water degreasing, decarbonization burning and sintering) was complicated. Subsequent work was undertaken using paraffin as injection binder and the degreasing process was simplified as very slow burning procedure. Via such modification, excellent piezoelectricity was acquired in the obtained BCHT ceramics, whereas their relative density decreased slightly.

In the aforementioned powder injection moulding method, the sintering temperature for preparation of the BCHT ceramics was still 1450 °C or above [17], making the ceramics processing cost expensive and difficult for manufacturing. Two techniques are well known to decrease sintering temperature effectively, i.e. using nano-sized precursor powder synthesized by wet chemical method or adding sintering aid. Ji *et al.* [18] obtained homogeneous high reactive $(Ba_{0.85}Ca_{0.15})(Zr_{0.1}Ti_{0.9})O_3$ precursor nanopowder by hydrothermal method, which decreases the sintering temperature to 1260 °C with elongating soaking time. Excellent ferroelectric, energy-storage and pyroelectric properties were obtained, and relative density higher than 94 %TD (theoretical density) and piezoelectric constant $d_{33}$ larger than 210 pC/N were obtained depending on sintering conditions. Sun *et al.* [19] studied the influence of $MnO_2$ addition on grain growth and electrical performance of $Ba_{0.98}Ca_{0.02}Zr_{0.02}Ti_{0.98}O_3$ ceramics. The ceramics sintered at 1400 °C has high relative density of 96.28 %TD, sharp dielectric peak at the Curie temperature of ~120 °C and rather large $d_{33}$ of 308 pC/N. In a similar system, Chen *et al.* [20] used $Li_2CO_3$ as sintering aid to fulfil low-temperature sintering of $(Ba_{0.85}Ca_{0.15})(Ti_{0.9}Zr_{0.1})O_3$ ceramics. The sintering temperature was decreased down to 1350 °C, whereas the relative density, still higher than 90 %TD and $d_{33} > 400$ pC/N was obtained. To form liquid phase during sintering and decrease sintering temperature effectively, it was recommended that the sintering aid should be added after calcination and the so-called two-step synthesis technique was adopted in ceramics preparation as clearly described in the study of Li-doped $(Ba_{0.85}Ca_{0.15})(Ti_{0.9}Zr_{0.1})O_3$ ceramics [20].

In this work, $(Ba_{0.85}Ca_{0.15})(Hf_{0.1}Ti_{0.9})O_3$ (BCHT) ceramics were prepared via the powder injection moulding using paraffin as injection binder and $MnO_2$ and $Li_2CO_3$ as sintering aids. $MnO_2$ and $Li_2CO_3$ were added into the raw materials together with other components and the injection precursor powders were obtained by calcination process. Such procedure will influence sintering process since solid solution is formed during the calcination process and ions mobility will be higher induced by heterovalent doping [21]. Detailed influences of Mn- and Li-doping on perovskite formation, grains morphology, electrical properties and ferroelectric characteristics were studied in detail.

## II. Experimental

The Mn- and Li-doped $(Ba_{0.85}Ca_{0.15})(Hf_{0.1}Ti_{0.9})O_3$ (BCHT) ceramics were prepared via the powder injection moulding using paraffin and oleic acid as injection binders [17,22]. Two different series with different amounts of sintering aids were obtained, i.e. in the first one with $MnO_2$ (Mn-BCHT-$x$, where $x$ indicates content of $MnO_2$ in mol% and $x$ = 0, 0.1, 0.3, 0.5, 1.0, 1.5, and 2.0) and the second one with $Li_2CO_3$ (Li-BCHT-$y$, where y indicates content of $Li_2CO_3$ in mol% and $y$ = 0, 0.4, 0.7, 1.0, 1.5, and 2.0). Stoichiometric amounts of $BaCO_3$ (99%), $CaCO_3$ (99%), $TiO_2$ (99.99%), $HfO_2$ (99.9%), $MnO_2$ (99.9%) and $Li_2CO_3$ (99.9%) were well mixed and calcined at 1350 °C for 3 h. The obtained precursor powders for injection moulding (81.5 vol.%) were mixed at 90 °C with 18 vol.% paraffin and 0.5 vol.% oleic acid. The injection binder was degreased via a very slow heating process using the 1250 °C calcined $Al_2O_3$ as adsorbent. Then, the degreased green pellets were sintered at 1450 °C for 4 h. Detailed powder injection moulding procedure was described in our previous work [17,22].

Phase structure of the polished Mn- and Li-doped BCHT ceramics was analysed by Rigaku D/max-2500/PC X-ray diffractometer. The relative density $\rho_r$ was calculated from bulk $\rho_{bulk}$ and theoretical $\rho_{theo}$ densities. The bulk density $\rho_{bulk}$ was measured by the Archimedes' water immersion method and the theoretical density $\rho_{theo}$ was calculated based on the cell volume obtained by the XRD measurement and chemical formula weight. Grains morphology of free surface of the sintered Mn- and Li-doped BCHT ceramics was observed by JEOL JSM-IT100 scanning electron microscope. For electrical performance measurement, silver electrode was coated by manual printing and fired at 650 °C for 30 min. Temperature dependent dielectric properties were measured by HDMS-1000 high-temperature dielectric measurement system. Large signal electric field induced polarization hysteresis (*P-E*) and strain loops (*S-E*) were detected by Precision Premier LC and AixACCT TF-analyzer 2000 ferroelectric testing system, respectively. For piezoelectricity characterization, the ceramics were poled using CS2674A withstand voltage tester under different electric fields at room temperature for 1 min. Piezoelectric constant $d_{33}$ was measured by ZJ-6A quasi-static piezoelectric tester. Planar electromechanical coupling coefficient $K_p$ and mechanical factor $Q_m$ were measured according to the IEEE standard using Agilent 4294A impedance analyser.

## III. Results and discussion

### 3.1. Phase structure characterization

XRD patterns of the Mn- and Li-doped BCHT ceramics are shown in Figs. 1 and 2, respectively. Rather pure perovskite structure is obtained in the BCHT ceramics with different amount of Mn- and Li-doping without detectable impurity. As shown in Figs. 1a and 2a, the ceramics can be indexed as pseudo-cubic structure since most diffraction peaks seem to be singlet peak with rather high symmetry on the whole within $2\theta$ of 10°-80° [23]. Such phenomena indicate that $Mn^{4+}/Mn^{2+}$ and $Li^{+}$ ions may diffuse into perovskite cell to form solid solution, which can be confirmed further based on the movement of diffraction peaks and the cell parameters calculation as discussed below.

As shown in Figs. 1b and 2b of the expanded XRD patterns around the {200} diffraction reflection, apparent splitting of the diffraction peak can be seen. With the variation of Mn- and Li-doping amount, the location ($2\theta$) of the respective diffraction peaks changes gradually, i.e. in both doping experiment the diffraction peaks tend to move to higher $2\theta$ degree with increasing the doping content. Such diffraction peaks' shift indicates the shrinkage of the crystalline cells, which can be attributed to the smaller radius of the doping cation during substitution process to form solid solution.

Complex site occupancies types exist in the Li-doped materials, including interstitial position and substitution at A- or B-site of the perovskite lattice. In this work, related cations radii are 1.61 Å, 1.34 Å and 1.18 Å for $Ba^{2+}$, $Ca^{2+}$ and $Li^{+}$ in 12-fold coordination and 0.71 Å, 0.605 Å and 0.76 Å for $Hf^{4+}$, $Ti^{4+}$ and $Li^{+}$ in 6-fold coordination, respectively [24,25]. Therefore, $Li^{+}$ tends to occupy A-site with large mobility and large off-centring as reported by Chen *et al.* [20], since Li occupying interstitial or B-site will lead to the expansion of the perovskite lattice.

As for the Mn-doped materials it is difficult to precisely determine whether Mn is located at A- or B-site of the perovskite structure. Both sites occupation may exist due to two reasons. The first, although $MnO_2$ was used as raw material, Mn tends to exist as $Mn^{4+}$ and $Mn^{2+}$ during sintering. Then, $Mn^{4+}$ and $Mn^{2+}$ tend to

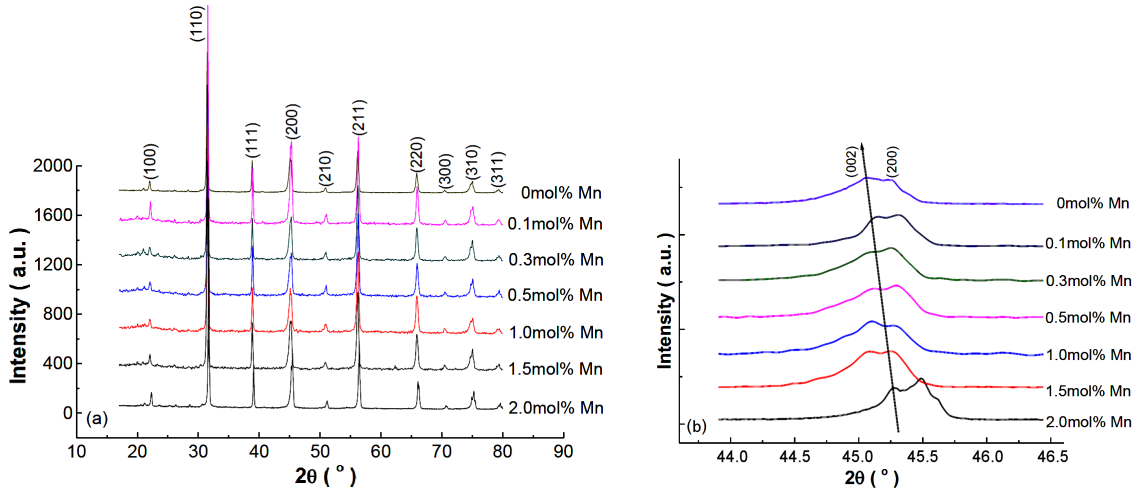


**Figure 1. XRD patterns of the Mn-BCHT-*x* ceramics sintered at 1450 °C (a) and expanded XRD patterns around {200} diffraction reflection (b)**

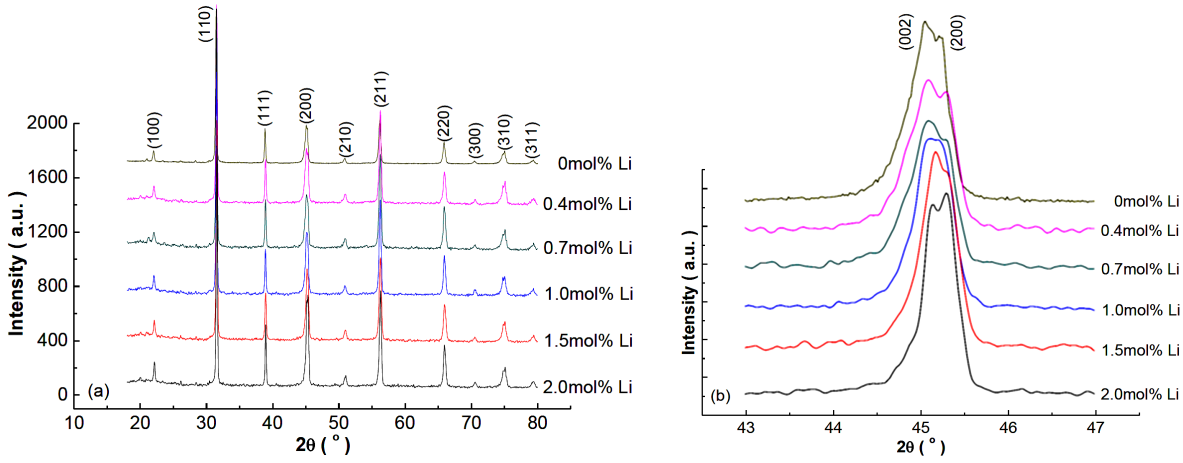


**Figure 2. XRD patterns of the Li-BCHT-*y* ceramics sintered at 1450 °C (a) and expanded XRD patterns around {200} diffraction reflection (b)**

occupy B-site and A-site of the perovskite structure due to its cation radii of 0.53 Å in 6-fold coordination and 0.96 Å in 8-fold coordination (in 12-fold coordination $Mn^{2+}$ ionic radius for A-site of the perovskite structure will be larger). Secondly, the calculated cell parameters of the Mn-doped BCHT ceramics change irregularly, which further confirm the complex site occupancy types existing in the Mn-doped BCHT ceramics considering the radii differences between $Ba^{2+}$, $Ca^{2+}$ and $Hf^{4+}$, $Ti^{4+}$ in respective coordination polyhedra.

With the increase of Mn- and Li-doping amounts, the relative intensity of the fitted (002) and (200) diffraction peaks reverses (Figs. 1b and 2b), correlating with the change of ferroelectric phases coexistence. In the study of the alkali niobate ceramics by Wu *et al.* [26], the intensity ratio of $I_{(002)}/I_{(200)}$ was used to determine phase structure, where 2:1 was regarded as orthorhombic (O) phase, 1:2 was attributed to tetragonal (T) phase and broadening of diffraction peaks and complex intensity ratio was considered as related to multi ferroelectric phases coexistence. Recently, Zhao *et al.* [4] revealed broad structural flexibility in a similar system $(1\text{-}x)Ba(Ti_{0.89}Sn_{0.11})O_3\text{-}x(Ba_{0.7}Ca_{0.3})TiO_3$, where multiphases convergence region with the coexistence of rhombohedral (R), O and T ferroelectric phases around cubic paraelectric phase zone was verified by XRD Rietveld refinement. Such existence was further observed inside nanodomains by atomic-resolution polarization mapping using aberration-corrected scanning transmission electron microscopy, contributing to the ultrahigh piezoelectricity [4]. Therefore, multi ferroelectric phases coexistence is confirmed, and the relative content of the T phase tends to increase with increasing the Mn- and Li-doping amounts according to the calculation method proposed by Wang *et al.* [27].

### *3.2. Density and grains micromorphology*

Due to the complicated ferroelectric phases coexistence in the BCHT system, the phase structure is indexed according to pseudo-cubic structure since most diffraction peaks present singlet nature in total (Table 1) [23]. It can be clearly seen that the Mn- and Li-doping increases densification of the BCHT ceramics, although adding dopant at the beginning would not decrease sintering temperature effectively, which can be attributed to the increase of ions mobility induced by doping [21]. It is proved that doping requires appropriate amount, where the Li-doping is more effective in the densification of the BCHT ceramics due to the largest relative density obtained with less doping amount. Considering the supposition of cell parameters calculation, lattice parameters present continuous decrease characteristic of the doped BCHT ceramics, confirming the formation of solid solution. As compared with the undoped BCHT ceramics prepared via powder injection moulding using paraffin as injection binder sintered at different temperatures, higher relative density >90 %TD is obtained via different amounts of Mn- and Li-doping sintered at 1450 °C, which increases their dielectric breakdown strength effectively. The largest densification is obtained in the Mn-BCHT-1.0 and Li-BCHT-0.7 ceramics, with relative density being 92.37 %TD and 93.05 %TD, respectively.

SEM images of the Mn- and Li-doped BCHT ceramics are shown in Figs. 3 and 4. Similar microstructural grain morphology characteristic can be found in both doped samples. Polyhedral grains combined with nearly round shape grains can be found, presenting the densification of liquid-phase sintering mechanism induced by the Mn- and Li-doping [21]. Bimodal distribution of grains can also be found in some ceramic samples, corroborating the difficulty of preparation of the BCB'T system ceramics due to the high sintering temperature [17]. The change of pores number corresponds well with the variation of density, which exerts effects on physical performance, but not significantly since grinding and polishing was undertaken before such measurement.

On the whole, clear grain boundary and compact grains are obtained in the doped BCHT ceramics. With the increase of Mn doping content, the average grain size tends to increase at first and then decreases with wave type variation, where the largest average grain size

**Table 1. Lattice parameters and density of the BCHT ceramics without doping and with different amounts of Mn- and Li-doping**

| Sample | $a = b = c$ [Å] | $\alpha = \beta = \gamma$ [°] | Cell volume [Å$^3$] | Bulk density [g/cm$^3$] | Relative density [%TD] |
|---|---|---|---|---|---|
| BCHT | 4.014 | 90.157 | 64.69 | 5.207 | 87.55 |
| Mn-BCHT-0.1 | 4.007 | 90.132 | 64.35 | 5.147 | 85.98 |
| Mn-BCHT-0.3 | 4.000 | 89.875 | 63.99 | 4.918 | 81.69 |
| Mn-BCHT-0.5 | 3.998 | 89.820 | 63.91 | 5.377 | 89.15 |
| Mn-BCHT-1.0 | 4.014 | 90.212 | 64.67 | 5.537 | 92.37 |
| Mn-BCHT-1.5 | 4.000 | 89.028 | 64.01 | 5.547 | 92.27 |
| Mn-BCHT-2.0 | 3.998 | 89.914 | 63.91 | 5.118 | 84.38 |
| Li-BCHT-0.4 | 4.016 | 90.206 | 64.76 | 5.469 | 92.03 |
| Li-BCHT-0.7 | 4.018 | 90.336 | 64.89 | 5.520 | 93.05 |
| Li-BCHT-1.0 | 4.015 | 90.220 | 63.74 | 5.287 | 88.90 |
| Li-BCHT-1.5 | 3.999 | 89.948 | 64.96 | 5.248 | 87.00 |
| Li-BCHT-2.0 | 4.011 | 90.132 | 64.53 | 5.307 | 88.94 |

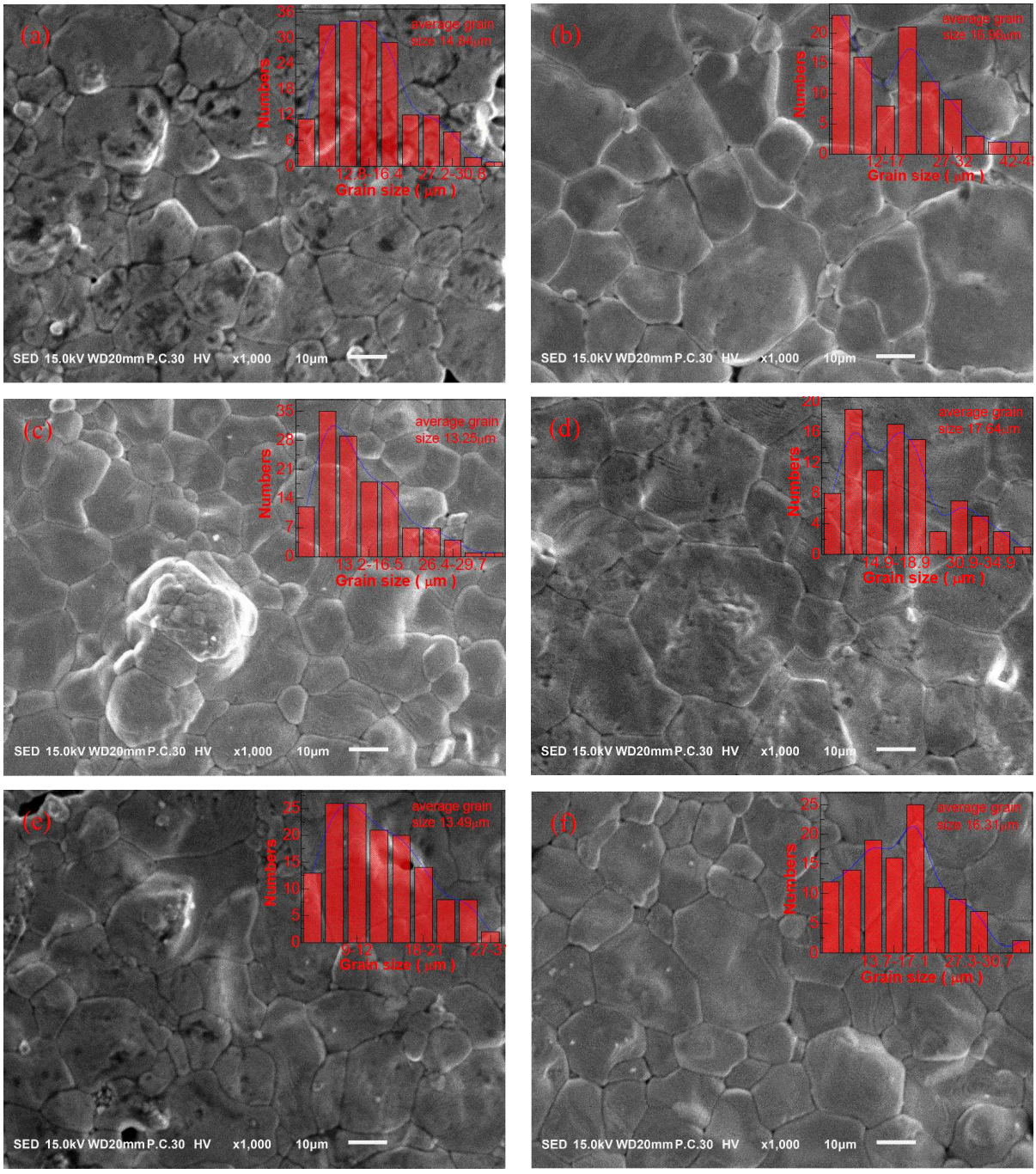


**Figure 3. SEM images of free surface of the Mn-BCHT-*x* ceramics after thermal etching at 1350 °C for 2 h: a) $x = 0.1$, b) $x = 0.3$, c) $x = 0.5$, d) $x = 1.0$, e) $x = 1.5$ and f) $x = 2.0$**

appears in the Mn-BCHT-1.0 ceramics, being 17.6 μm. As comparison, maximum average grain size is obtained in the Li-doped samples, where the average grain size increases at first and then decreases with increasing the Li-doping content, and the Li-BCHT-0.7 ceramic sample has the maximum average grain size of 20.4 μm.

With the change of Mn- and Li-doping amount, grains size and distribution, pores number and ceramics density change accordingly. The major densification mechanism can be attributed to the formation of cationic point defects and oxygen vacancies via different processes [28]:

$$Mn^{2+} \xrightarrow{Hf^{4+}/Ti^{4+}} Mn''_{Hf/Ti} + V_O^{\bullet\bullet} \quad (1)$$

$$2\,Mn^{3+} \xrightarrow{Hf^{4+}/Ti^{4+}} 2\,Mn'_{Hf/Ti} + V_O^{\bullet\bullet} \quad (2)$$

$$2\,Li^{+} \xrightarrow{Ba^{2+}/Ca^{2+}} 2\,Li'_{Ba/Ca} + V_O^{\bullet\bullet} \quad (3)$$

For low heterovalent cations substitution of Mn substituting $Hf^{4+}/Ti^{4+}$ and Li substituting $Ba^{2+}/Ca^{2+}$, oxygen vacancies are generated to compensate charge balance [19,29,30]. Such point defects increase mobility of ions, which increases ceramics densification and grains size

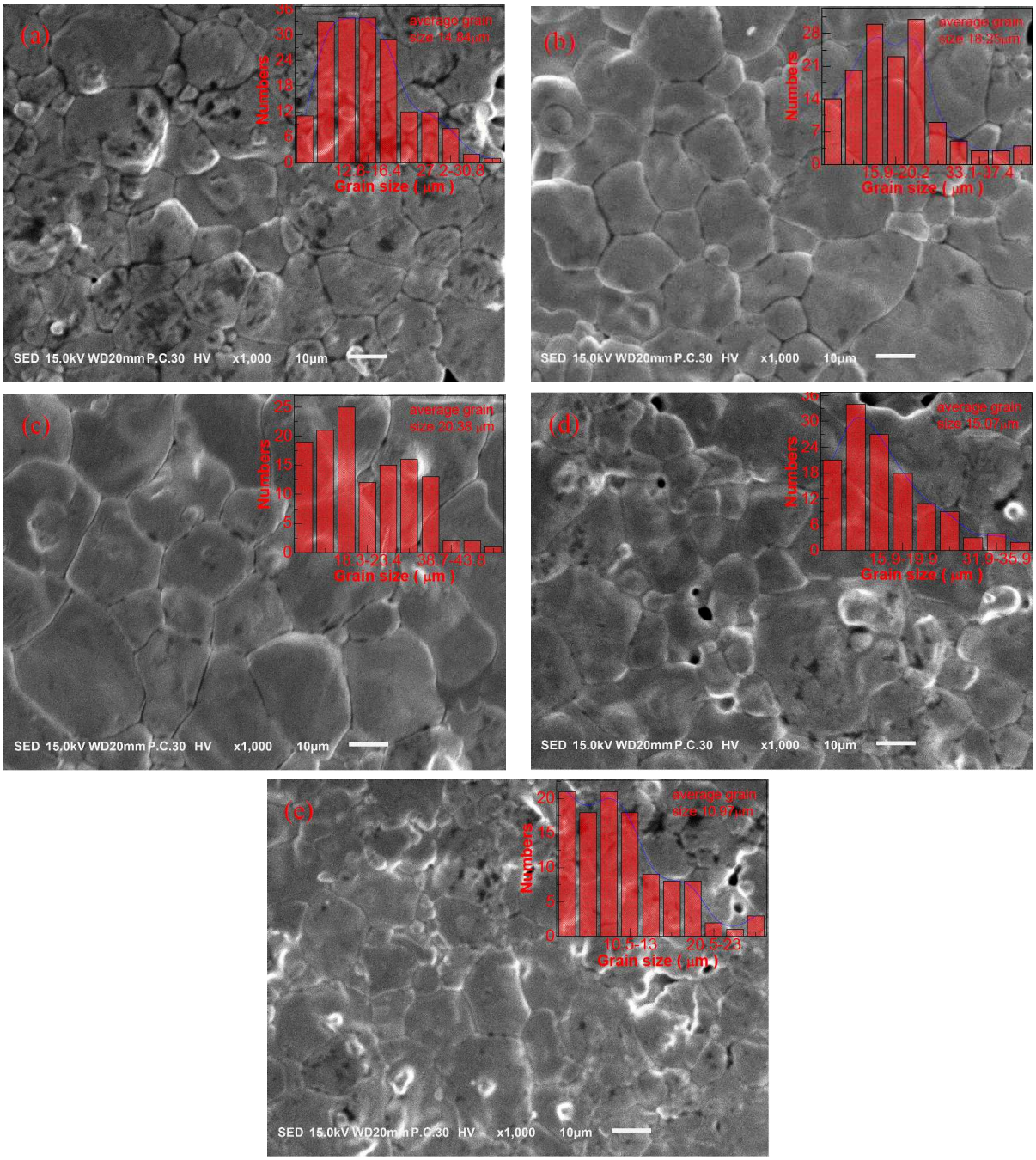


**Figure 4. SEM images of free surface of the Li-BCHT-*y* ceramics after thermal etching at 1350 °C for 2 h: a) $y = 0.4$, b) $y = 0.7$, c) $y = 1.0$, d) $y = 1.5$ and e) $y = 2.0$**

although the amount of liquid phase produced during sintering also exerts impact. Whereas, when the doping content is excessive, grain growth is inhibited accompanied by irregular change of grains morphology [21].

### *3.3. Dielectric properties and ferroelectric nature*

Figure 5 shows dielectric performance of the Mn- and Li-doped BCHT ceramics. Sole dielectric peak around the Curie temperature ($T_C$) is observed in all samples, which correlates with the MPB ferroelectric phase to cubic paraelectric phase transition [10]. Relative density and grains morphology are major factors affecting dielectric properties, which vary with the doping content. As shown in Fig. 5a, as compared with the undoped BCHT ceramics, dielectric constant maximum ($\varepsilon_m$) increases slightly and dielectric peak becomes sharper at first, and then the $\varepsilon_m$ value decreases greatly and dielectric peak broadens quickly accompanied by the variation of the $T_C$ temperature. Dielectric loss decreases slightly at first and then increases slightly with increasing the Mn-doping content. In the Li-doped BCHT ceramics, dielectric constant presents similar change trend with more apparent regularity with increasing the Li-doping content. Furthermore, dielectric loss decreases in all samples (Fig. 5b). The low-temperature shoulder appeared in the loss tangent-temperature curves corre-

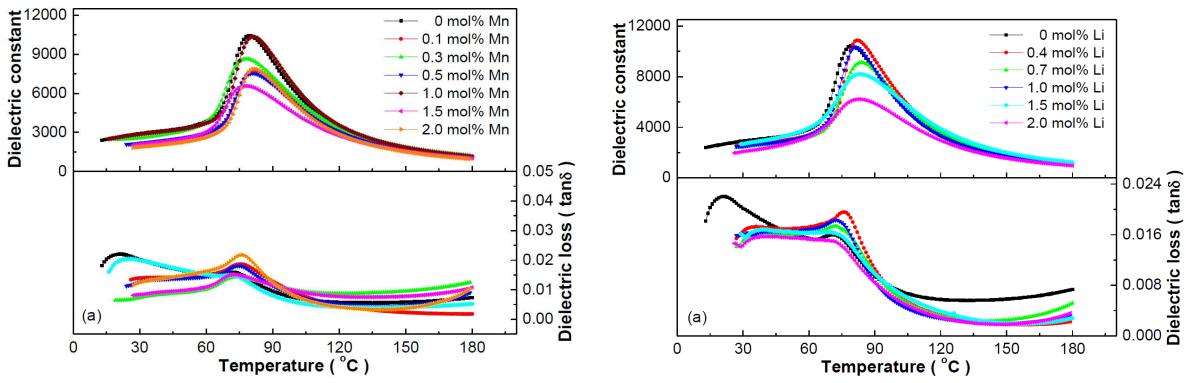


**Figure 5. Temperature dependent dielectric performance of: a) Mn-BCHT-*x* and b) Li-BCHT-*y* ceramics measured upon heating at 10 kHz**

lating with the polymorphic ferroelectric phase transition [10].

The influence of frequency on dielectric performance is shown in Figs. 6a and 6b using the Mn-BCHT-1.0 and Li-BCHT-0.4 ceramics as examples. Almost the largest dielectric constant value, being $\varepsilon_m$ = 10556 with $T_C$ = 81 °C and $\varepsilon_m$ = 11154 with $T_C$ = 82 °C at 1 kHz, respectively, and narrow dielectric peaks are obtained in these ceramics, correlating with the large relative density and appropriate grains size. The multi ferroelectric phases coexistence also contributes to the excellent dielectric performance [4].

Ferroelectric characteristic of the Mn- and Li-doped BCHT ceramics can be studied via dielectric behaviour fitted by the Curie-Weiss law and exponential law as shown in Fig. 7 using the Mn-BCHT-1.0 and Li-BCHT-0.4 ceramics as examples [31,32]. Based on the dielectric response fitting, the fitted equations are $\varepsilon$ =

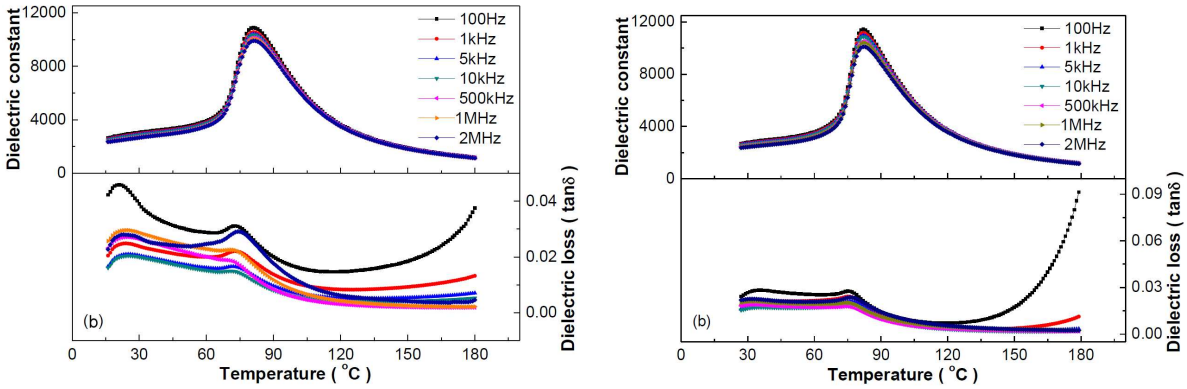


**Figure 6. Frequency dependent dielectric performance of: a) Mn-BCHT-1.0 and b) Li-BCHT-0.4 ceramics measured upon heating**

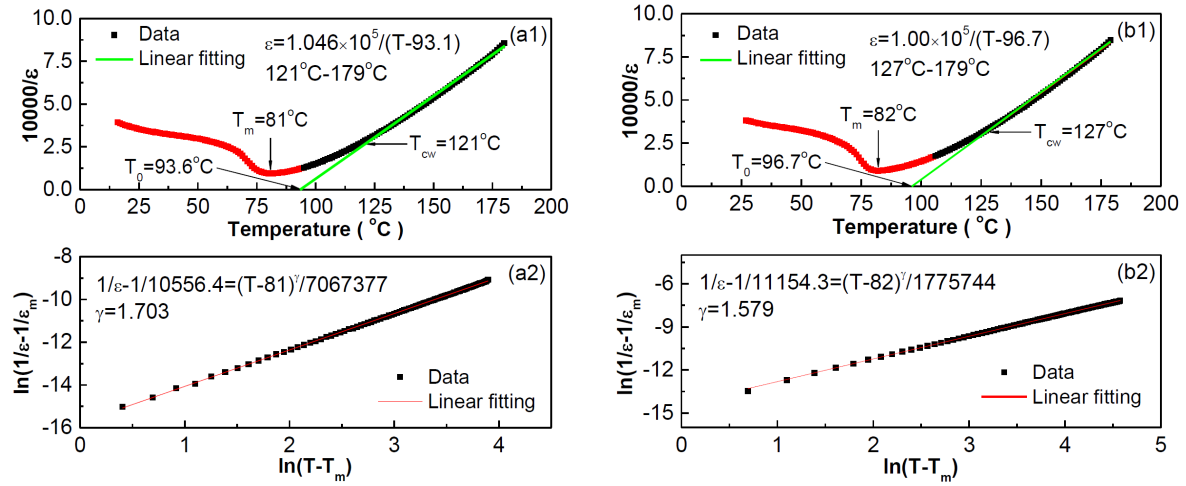


**Figure 7. Dielectric behaviour fitting of: a) Mn-BCHT-1.0 and b) Li-BCHT-0.4 ceramics using the Curie-Weiss (1) and exponential law (2)**

$1.046 \times 10^5/(T - 93.1)$ and $1/\varepsilon - 1/10556.4 = (T - 81)^{1.703}/7067377$ for the Mn-BCHT-1.0 ceramics, and $\varepsilon = 1.00 \times 10^5/(T - 96.7)$ and $1/\varepsilon - 1/11154.3 = (T - 82)^{1.579}/1775744$ for the Li-BCHT-0.4 ceramics, respectively. All the ceramics can be fitted by both laws, but all have deviations to some extent. The fitted Curie-Weiss constant $C$ is around $10^5$, correlating with normal ferroelectrics characteristic [31]. The diffusive coefficient $\gamma$ is close to 2 in the Mn-doped BCHT ceramics, and the $\gamma$ value is larger than 1.5 in all samples, revealing partial relaxor ferroelectrics nature [31,32]. Therefore, the Mn- and Li-doped BCHT ceramics are displacement driven ferroelectrics with apparent diffused characteristic to some extent, related to the MPB composition selected and the variation of point defects induced by different doping content [33].

### 3.4. Ferroelectric and strain performance

Figures 8 and 9 show ferroelectric and strain properties of the Mn-BCHT-$x$ ceramics. Rather saturated and enhanced symmetric $P$-$E$ hysteresis loops are obtained in the doped BCHT ceramics. With the increase of Mn-doping content, remnant polarization $P_r$ tends to decrease and coercive field $E_c$ tends to increase with variant change. Within the Mn-doping amount of 0–0.3 mol% and 1.0–2.0 mol%, the $P_r$ value decreases due to the pinning down effect on the ferroelectric domains induced by point defects and their aggregation [34]; whereas, within 0.3–1.0 mol% Mn-doping amount, the increase of relative density and grains size compensate such decrease to some extent, leading to slight increase of the $P_r$ value. Excellent ferroelectricity is obtained in the Mn-BCHT-1.0 ceramics, with $P_r = 8.81\,\mu C/cm^2$ and $E_c = 3.7$ kV/cm. The Mn-BCHT-2.0 ceramics shows rather symmetric butterfly-like $S$-$E$ loop (Fig. 9), and the strain reaches 0.1% at only 25 kV/cm far less than saturation. The inverse piezoelectric constant $d^*_{33} = 404.2$ pm/V and strain hysteresis of 8.01% are calculated according to literature reported method [35].

Ferroelectric and strain properties of the Li-BCHT-$y$ ceramics are shown in Figs. 10 and 11. Similar ferroelectric and strain behaviour can be found with some difference. When the Li-doping amount is above 1.5 mol%, the $P_r$ value decreases sharply; whereas the $E_c$ value increases slightly with elevating the Li-doping content. As discussed above, point defect $Li'_{Ba/Ca}$ forms due to doping, then $V_O^{\bullet\bullet}$ is generated to compensate charge balance [28]. Such point defects and their ag-

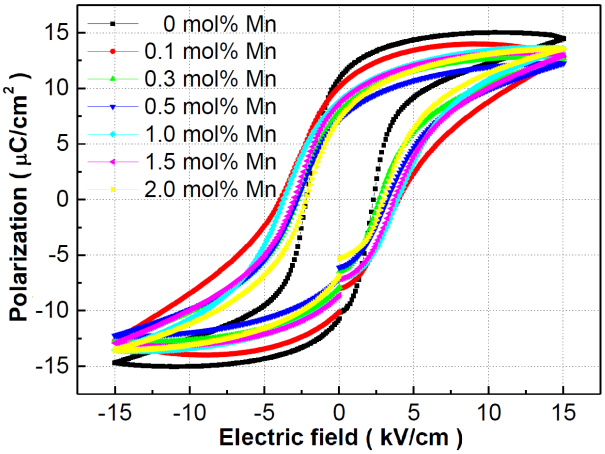


**Figure 8. $P$-$E$ hysteresis loops of the Mn-BCHT-$x$ ceramics measured at 15 kV/cm and 1 Hz**

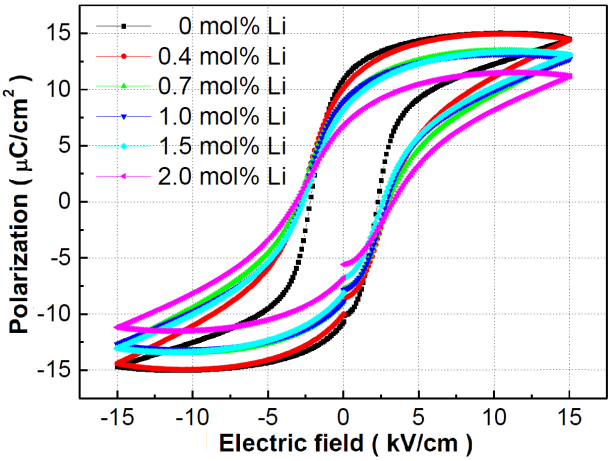


**Figure 10. $P$-$E$ hysteresis loops of the Li-BCHT-$y$ ceramics measured at 15 kV/cm and 1 Hz**

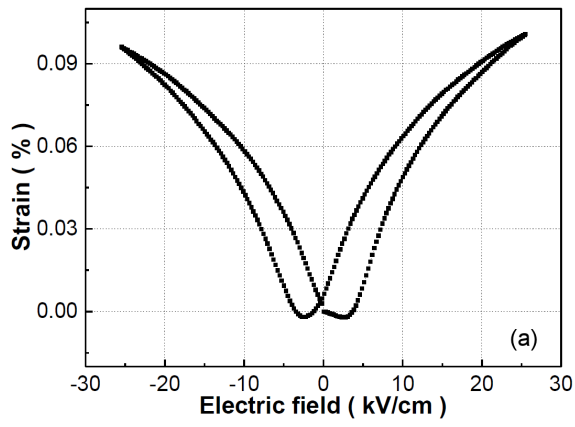


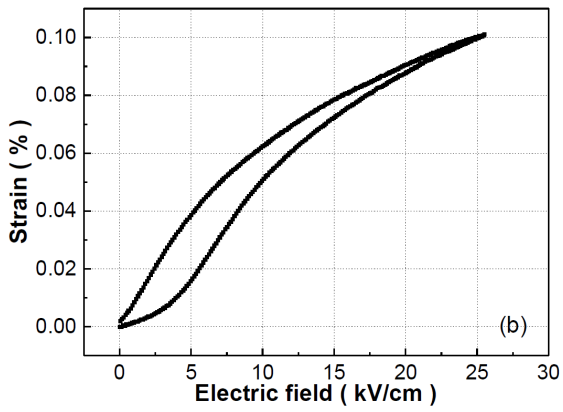


**Figure 9. Bipolar (a) and unipolar (b) $S$-$E$ loops of the Mn-BCHT-2.0 ceramics measured at 25 kV/cm and 10 Hz around room temperature**

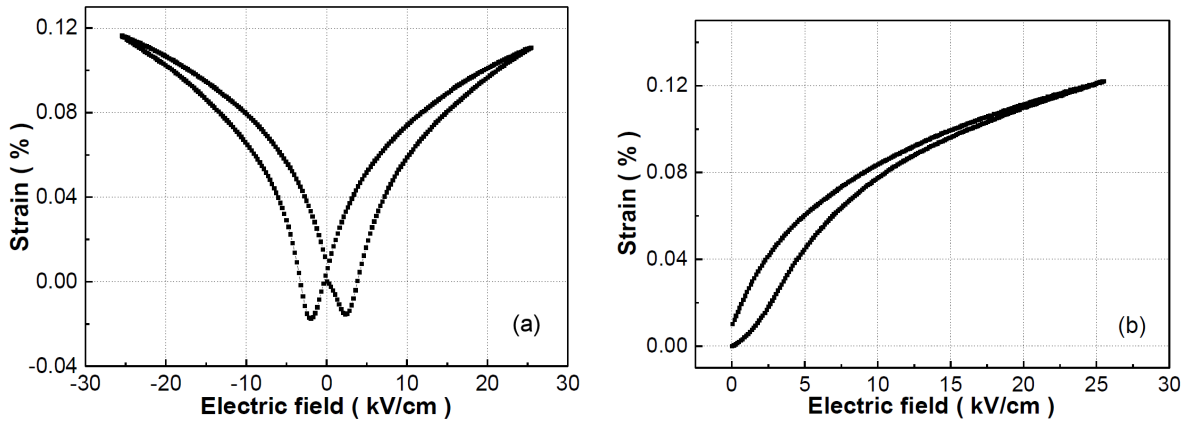


**Figure 11. Bipolar (a) and unipolar (b) *S-E* loops of the Li-BCHT-0.4 ceramics measured at 25 kV/cm and 10 Hz around room temperature**

gregation pins down the mobility of ferroelectric domains, leading to the decrease of $P_r$ value and increase of $E_c$ value with different influence extent [34]. When compared with the Mn-BCHT-2.0 ceramics, higher $P_r$ of 10.04 μC/cm$^2$, lower $E_c$ of 3.0 kV/cm, as well as increased strain to 0.122% at only 25 kV/cm without saturation (Fig. 11) are obtained. Also, increased inverse piezoelectric constant $d^*_{33}$ = 488.4 pm/V and decreased strain hysteresis of 3.15% [35] are obtained for the Li-BCHT-0.4 ceramics.

### 3.5. Piezoelectric property

Poling condition is major factor influencing piezoelectricity of piezoelectric materials [36], where Fig. 12 shows the effect of poling electric field on the piezoelectric properties of the Mn- and Li-doped BCHT ceramics. As compared with the undoped BCHT ceramics, the Mn- and Li-doped BCHT ceramics present easy polarization characteristic and piezoelectric constant $d_{33}$ increases slightly with increasing electric field due to the introduction of point defects via doping. For the Mn-doped BCHT ceramics, the $d_{33}$ value decreases at first and then increases with increasing the Mn-doping amount, and the minimum $d_{33}$ value appears in the Mn-BCHT-1.0 ceramics. For the Li-doped BCHT ceramics, when the Li-doping content is above 1.0 mol%, the $d_{33}$ value decreases sharply, before which the $d_{33}$ value of the Li-doped BCHT ceramics is larger than 300 pC/N. Such $d_{33}$ value change can be attributed to the complex influences of crystalline related factors including pores, density and grains size and distribution, and concentration of moveable $V_O^{\bullet\bullet}$. The average grains size and relative density increase at first and then decrease with the increase of doping content due to the competition between liquid-phase sintering mechanism contribution and inhibition of grain growth with excessive doping amount. Besides, point defects of $Mn''_{Hf/Ti}$, $Mn'_{Hf/Ti}$ and $Li'_{Ba/Ca}$ are formed induced by Mn- and Li-doping, and $V_O^{\bullet\bullet}$ is generated for charge balance compensation [28]. Such point defects and their aggregation increase ions mobility and prevent ferroelectric domains movement [19,34] depending on the concentration. Table 2 shows the influence of poling electric field on the planar electromechanical coupling coefficient $K_p$ and mechanical factor $Q_m$ of the Mn- and Li-doped BCHT ceramics. Similar change trend of $K_p$ appears in the ceramics, and rather large $K_p$ value can be obtained at appropriate doping amount.

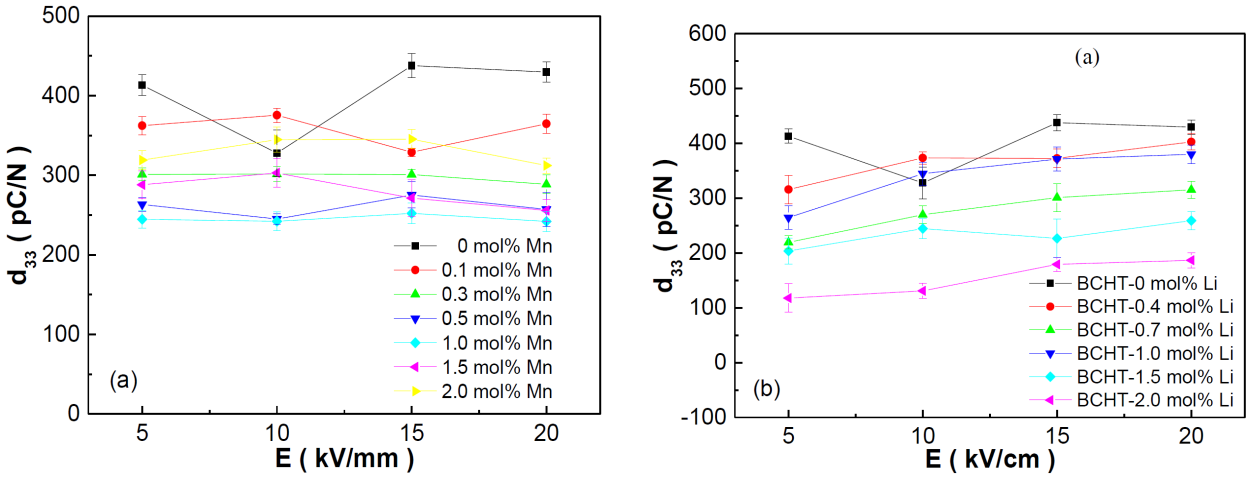


**Figure 12. Electric field dependence of piezoelectricity of: a) Mn-BCHT-*x* and b) Li-BCHT-*y* ceramics**

**Table 2. $K_p$ and $Q_m$ of the BCHT ceramics without doping and with different Mn- and Li-doping contents under different poling electric field**

| Doping type and content | $K_p$ | | | | $Q_m$ | | | |
|---|---|---|---|---|---|---|---|---|
| | 5 kV/cm | 10 kV/cm | 15 kV/cm | 20 kV/cm | 5 kV/cm | 10 kV/cm | 15 kV/cm | 20 kV/cm |
| BCHT | 0.338 | 0.336 | 0.372 | 0.395 | 3903 | 719 | 495 | 432 |
| Mn-BCHT-0.1 | 0.302 | 0.309 | 0.325 | 0.313 | 162 | 203 | 185 | 173 |
| Mn-BCHT-0.3 | 0.265 | 0.274 | 0.286 | 0.273 | 262 | 223 | 284 | 54 |
| Mn-BCHT-0.5 | 0.251 | 0.255 | 0.259 | 0.253 | 962 | 666 | 713 | 613 |
| Mn-BCHT-1.0 | 0.121 | 0.122 | 0.127 | 0.127 | 67 | 84 | 32 | 78 |
| Mn-BCHT-1.5 | 0.277 | 0.276 | 0.275 | 0.264 | 721 | 679 | 796 | 995 |
| Mn-BCHT-2.0 | 0.302 | 0.325 | 0.320 | 0.308 | 401 | 459 | 384 | 421 |
| Li-BCHT-0.4 | 0.294 | 0.335 | 0.354 | 0.368 | 152 | 128 | 128 | 150 |
| Li-BCHT-0.7 | 0.214 | 0.273 | 0.310 | 0.372 | 150 | 157 | 148 | 140 |
| Li-BCHT-1.0 | 0.239 | 0.296 | 0.322 | 0.334 | 162 | 155 | 152 | 151 |
| Li-BCHT-1.5 | 0.193 | 0.232 | 0.207 | 0.243 | 137 | 138 | 122 | 130 |
| Li-BCHT-2.0 | 0.214 | 0.226 | 0.211 | 0.232 | 42 | 59 | 117 | 88 |

## IV. Conclusions

The Mn- and Li-doped BCHT ceramics were prepared via powder injection moulding using paraffin as injection binder. Rather pure perovskite structure is obtained in the doped BCHT ceramics, where multi ferroelectric phases coexist with different content depending on the Mn- and Li-doping amount. Via Mn- and Li-doping, average grains size increases and relative density can be larger than 90 %TD, where the largest average grains size appears in the Mn-BCHT-1.0 ceramics and Li-BCHT-0.7 ceramics, being 17.6 μm and 20.4 μm, and the largest densification is obtained in the Mn-BCHT-1.0 and Li-BCHT-0.7 ceramics, with relative density being 92.37 and 93.05 %TD, respectively. The Mn- and Li-doped BCHT ceramics are displacement driven ferroelectrics with apparent diffused characteristic to a different extent. Excellent ferroelectricity is obtained in the Mn-BCHT-1.0 ceramics, with $P_r$ = 8.81 μC/cm$^2$ and $E_c$ = 3.7 kV/cm. The strain reaches 0.1% at only 25 kV/cm, inverse piezoelectric constant is $d^*_{33}$ = 404.2 pm/V and strain hysteresis is 8.01% for the Mn-BCHT-2.0 ceramics. For the Li-BCHT-0.4 ceramics, $P_r$ is 10.04 μC/cm$^2$, $E_c$ is 3.0 kV/cm, strain reaches 0.122% at only 25 kV/cm, $d^*_{33}$ = 488.4 pm/V and strain hysteresis is 3.15%. The Mn- and Li-doped BCHT ceramics present easy polarization characteristic, and the $d_{33}$ value larger than 300 pC/N can be obtained at appropriate doping amount.

**Acknowledgements:** The authors thank the National Natural Science Foundation of China (No. 51577015), the Top-notch Academic Programs Project of Jiangsu Higher Education Institutions and the Priority Academic Program Development of Jiangsu Higher Education Institutions for financial support.

## References

1. N. Zhang, H. Yokota, A.M. Glazer, Z. Ren, D.A. Keen, D.S. Keeble, P.A. Thomas, Z.-G. Ye, "The missing boundary in the phase diagram of $PbZr_{1-x}Ti_xO_3$", *Nature Commun.*, **5** (2014) 5231.
2. B. Narayan, J.S. Malhotra, R. Pandey, K. Yaddanapudi, P. Nukala, B. Dkhil, A. Senyshyn, R. Ranjan, "Electrostrain in excess of 1% in polycrystalline piezoelectrics", *Nature Mater.*, **17** (2018) 427–431.
3. J. Zeng, K. Zhao, X. Shi, X. Ruan, L. Zheng, G. Li, "Large strain induced by the alignment of defect dipoles in $(Bi^{3+},Fe^{3+})$ co-doped $Pb(Zr,Ti)O_3$ ceramics", *Scripta Mater.*, **142** (2018) 20–22.
4. C. Zhao, H. Wu, F. Li, Y. Cai, Y. Zhang, D. Song, J. Wu, X. Lyu, J. Yin, D. Xiao, J. Zhu, S.J. Pennycook, "Practical high piezoelectricity in barium titanate ceramics utilizing multiphase convergence with broad structural flexibility", *J. Am. Chem. Soc.*, **140** (2018) 15252–15260.
5. Y. Wang, C. Luo, S. Wang, C. Chen, G. Yuan, H. Luo, D. Viehland, "Large piezoelectricity in ternary lead-free single crystals", *Adv. Electron. Mater.*, **6** [1] (2020) 1900949.
6. X. Lv, J. Zhu, D. Xiao, X.-X. Zhang, J. Wu, "Emerging new phase boundary in potassium sodium-niobate based ceramics", *Chem. Soc. Rev.*, **49** (2020) 671–707.
7. W. Liu, X. Ren, "Large piezoelectric effect in Pb-free ceramics", *Phys. Rev. Lett.*, **103** (2009) 257602.
8. C. Zhou, W. Liu, D. Xue, X. Ren, H. Bao, J. Gao, L. Zhang, "Triple-point-type morphotropic phase boundary based large piezoelectric Pb-free material-$Ba(Ti_{0.8}Hf_{0.2})O_3$-$(Ba_{0.7}Ca_{0.3})TiO_3$", *Appl. Phys. Lett.*, **100** [22] (2012) 222910.
9. S. Chootin, T. Bongkarn. "Optimum conditions for preparation of high-performance $(Ba_{0.97}Ca_{0.03})(Ti_{0.94}Sn_{0.06})O_3$ ceramics by solid-state combustion", *J. Electron. Mater.*, **46** [8] (2017) 5215–5224.
10. D.S. Keeble, F. Benabdallah, P.A. Thomas, M. Maglione, J. Kreisel, "Revised structural phase diagram of $(Ba_{0.7}Ca_{0.3}TiO_3)$-$(BaZr_{0.2}Ti_{0.8}O_3)$", *Appl. Phys. Lett.*, **102** (2013) 092903.
11. M.B. Abdessalem, S. Aydi, A. Aydi, N. Abdelmoula, Z. Sassi, H. Khemakhem, "Polymorphic phase transition and morphotropic phase boundary in $Ba_{1-x}Ca_xTi_{1-y}Zr_yO_3$ ceramics", *Appl. Phys. A*, **123** (2017) 583.
12. C. Zhao, W. Wu, H. Wang, J. Wu, "Site engineering and polarization characteristics in $(Ba_{1-y}Ca_y)(Ti_{1-x}Hf_x)O_3$ lead-free ceramics", *J. Appl. Phys.*, **119** (2016) 024108.
13. S. Zhang, B. Fang, X. Zhao, S. Zhang, Z. Chen, J. Ding, "Multifunctional performance derived by Eu doping in $(Ba_{0.85}Ca_{0.15})(Ti_{0.9}Hf_{0.1})O_3$ lead-free ceramics", *J. Mater.*

*Sci. Mater. Electron.*, **30** [21] (2019) 19404–19414.
14. L. Liu, "Progress on the fabrication of lead-free textured piezoelectric ceramics: Perspectives over 25 years", *J. Mater. Sci. Mater. Electron.*, **26** (2015) 4425–4437.
15. R. Zhu, Q. Zhang, B. Fang, D. Wu, X. Zhao, J. Ding, "Correlation of enhanced electrical properties and domain structure of high-$T_C$ PMN-PH-PT ceramics prepared by different methods", *Ceram. Int.*, **44** [9] (2018) 10099–10105.
16. K.J. Shree, D. Das, "Molten salt assisted growth of lead-free BCZT crystals: effects of synthesis conditions and sintering on structural and electrical properties", *J. Mater. Sci. Mater. Electron.*, **30** (2019) 11094–11107.
17. C. Wang, D. Wu, B. Fang, S. Zhang, J. Ding, "Preparation and electrical performance of BCHT lead-free piezoelectric ceramics via powder injection molding", *Ferroelectrics*, **558** [1] (2020) 12–26.
18. W. Ji, B. Fang, X. Lu, S. Zhang, N. Yuan, J. Ding, "Tailoring structure and performance of BCZT ceramics prepared via hydrothermal method", *Physica B*, **567** (2019) 65–78.
19. H. Sun, S. Duan, X. Liu, D. Wang, H. Sui, "Lead-free $Ba_{0.98}Ca_{0.02}Zr_{0.02}Ti_{0.98}O_3$ ceramics with enhanced electrical performance by modifying $MnO_2$ doping content and sintering temperature", *J. Alloys Compd.*, **670** (2016) 262–267.
20. X. Chen, X. Ruan, K. Zhao, X. He, J. Zeng, Y. Li, L. Zheng, C.H. Park, G. Li, "Low sintering temperature and high piezoelectric properties of Li-doped (Ba,Ca)(Ti,Zr)$O_3$ lead-free ceramics", *J. Alloys Compd.*, **632** (2015) 103–109.
21. R.M. German, P. Suri, S.J. Park, "Review: Liquid phase sintering", *J. Mater. Sci.*, **44** (2009) 1–39.
22. D. Wu, S. Qin, C.-L. Liu, B.-J. Fang, Z. Cao, J.-F. Cheng, "Surface modification by stearic acid on property of PLZT piezoelectric ceramics prepared via powder injection molding", *J. Inorg. Mater.*, **34** [5] (2019) 535–540 (in Chinese).
23. Y. Zhang, H. Sun, W. Chen, "A brief review of $Ba(Ti_{0.8}Zr_{0.2})O_3$-$(Ba_{0.7}Ca_{0.3})TiO_3$ based lead-free piezoelectric ceramics: Past, present and future perspectives", *J. Phys. Chem. Solids*, **114** (2018) 207–219.
24. R.D. Shannon, "Revised effective ionic radii and systematic studies of interatomic distances in halides and chalcogenides", *Acta Crystallograph. A*, **32** (1976) 751–767.
25. T. Kimura, Q. Dong, S. Yin, T. Hashimoto, A. Sasaki, T. Sato, "Synthesis and piezoelectric properties of Li-doped $BaTiO_3$ by a solvothermal approach", *J. Eur. Ceram. Soc.*, **33** (2013) 1009–1015.
26. B. Wu, H. Wu, J. Wu, D. Xiao, J. Zhu, S. J. Pennycook, "Giant piezoelectricity and high curie temperature in nanostructured alkali niobate lead-free piezoceramics through phase coexistence", *J. Am. Chem. Soc.*, **138** (2016) 15459–15464.
27. K. Wang, J.-F. Li. "Domain engineering of lead-free Li-modified (K,Na)$NbO_3$ polycrystals with highly enhanced piezoelectricity", *Adv. Funct. Mater.*, **20** (2010) 1924–1929.
28. F.A. Kröger, H.J. Vink, "Relations between the concentrations of imperfections in crystalline solids", *Solid State Phys.*, **3** (1956) 307–435.
29. F. Fen, Y. Yan, "Large electrostrictive effect in Mn-doped BCZT ferroelectric ceramics", *Ceram. Int.*, **45** (2019) 21315–21320.
30. Y. Zhang, H. Sun, W. Chen. "Li-modifified $Ba_{0.99}Ca_{0.01}Zr_{0.02}Ti_{0.98}O_3$ lead-free ceramics with highly improved piezoelectricity", *J. Alloy. Compd.*, **649** (2017) 745–751.
31. V.V. Shvartsman, W. Kleemann, J. Dec, Z. K. Xu, S. G. Lu, "Diffuse phase transition in $BaTi_{1-x}Sn_xO_3$ ceramics: An intermediate state between ferroelectric and relaxor behavior", *J. Appl. Phys.*, **99** [12] (2006) 124111.
32. K. Uchino, S. Nomura, "Critical exponents of the dielectric constants in diffused-phase-transition crystals", *Ferroelectr. Lett.*, **44** (1982) 55–61.
33. F.-Z. Yao, K. Wang, W. Jo, K.G. Webber, T.P. Comyn, J.-X. Ding, B. Xu, L.-Q. Cheng, M.-P. Zheng, Y.-D. Hou, J.-F. Li, "Diffused phase transition boosts thermal stability of high-performance lead-free piezoelectrics", *Adv. Funct. Mater.*, **26** [8] (2016) 1217–1224.
34. H. Sun, Y. Zhang, X. Liu, Y. Liu, S. Guo, W. Chen, "Effects of cobalt and sintering temperature on electrical properties of $Ba_{0.98}Ca_{0.02}Zr_{0.02}Ti_{0.98}O_3$ lead-free ceramics", *J. Mater. Sci. Mater. Electron.*, **25** (2014) 3962–3966.
35. D. Wang, M. Cao, S. Zhang, "Investigation of ternary system $PbHfO_3$-$PbTiO_3$-$Pb(Mg_{1/3}Nb_{2/3})O_3$ with morphotropic phase boundary compositions", *J. Am. Ceram. Soc.*, **95** (2012) 3220–3228.
36. H. Wan, C. Luo, W.-Y. Chang, Y. Yamashita, X. Jiang, "Effect of poling temperature on piezoelectric and dielectric properties of $0.7Pb(Mg_{1/3}Nb_{2/3})O_3$-$0.3PbTiO_3$ single crystals under alternating current poling", *Appl. Phys. Lett.*, **114** (2019) 172901.